Macromolecules

pubs.acs.org/Macromolecules Article

Decoupled Cation Transport within Layered Assemblies in Sulfonated and Crystalline Telechelic Polyethylenes

Benjamin A. Paren, Manuel Häußler, Patrick Rathenow, Stefan Mecking,* and Karen I. Winey*

Cite This: *Macromolecules* 2022, 55, 2813−2820 Read Online

ACCESS | Metrics & More | Article Recommendations | Supporting Information

ABSTRACT: We present a set of sulfonated monodisperse telechelic polyethylene ionomers that demonstrate ion transport of metal cations in layered ionic assemblies. These semicrystalline ionomers have precisely 48 backbone carbons with a sulfonated group at each end and are fully neutralized by a counterion, $C_{48}(SO_3X)_2$ (X = Li^+ or Na^+). The morphology of these polymers is characterized by using X-ray scattering, and ionic conductivity is probed by using electrochemical impedance spectroscopy. These telechelic polyethylenes exhibit well-defined ionic layers at all temperatures below the melting point, and the crystal packing of the backbone varies with temperature. The polyethylene backbone packs in hexagonal crystals at high temperatures in both $C_{48}(SO_3Li)_2$ and $C_{48}(SO_3Na)_2$, with Arrhenius activation energies (E_a) for ion transport of 120 and 53 kJ mol^{-1}, respectively, indicating that decoupled ion transport is possible through these layered ionic assemblies. The E_a in this hexagonal regime is significantly lower than E_a at room temperature where $C_{48}(SO_3Li)_2$ exhibits disordered crystals and $C_{48}(SO_3Na)_2$ exhibits orthorhombic crystallites, highlighting the impact of polymer packing between the ionic layers. At intermediate temperatures (120−160 °C) the hexagonal crystal structure in $C_{48}(SO_3Na)_2$ coexists with an unidentified crystal phase that appears to have superior ion transport properties. When compared to other single ion conductors of the same functionality, $C_{48}(SO_3Na)_2$ also demonstrates the importance of ionic assembly shape and identifies ionic layers as a promising strategy relative to assemblies with less order.

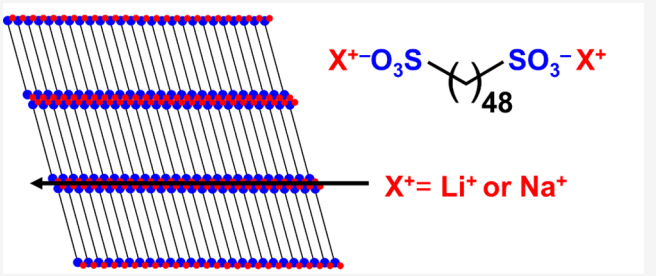

INTRODUCTION

Developing solid polymer electrolytes (SPEs) with high ion conductivity is of key interest due to their improved safety and mechanical stability over liquid electrolytes.[1−4] Single-ion conducting polymers are a class of solid polymer electrolytes that have anion functional groups covalently bonded to the polymer, and thus the mobility of the cation is much greater than the anion, thereby increasing the transference number.[4] A variety of nanoscale morphologies have been identified in functionalized polymers that merit exploring for alternative ion transport mechanisms in solid polymer electrolytes. Recent work by Sokolov and co-workers discussed that aggregate morphologies that are more favorable for correlated chain-like ion jumps could significantly increase the total charge transport in a solid polymer electrolyte, specifically in single-ion conductors.[3,5] This suggests that planar or layered assemblies could similarly improve ion transport compared to the discrete or disordered aggregates present in typical amorphous single-ion conducting polymers.[3,6]

Precise polyethylene-based single-ion conductors form layered ionic assemblies when the alkane spacer is long enough to crystallize.[7−16] This class of polymers was initially synthesized by acyclic diene metathesis (ADMET),[17] and these precise polymers form layers with a variety of functional groups, including various acids, imidazolium, halides, and polyacetals.[7−16] A variety of polyethylene backbone crystal structures exist between the layers, depending on the functional group, backbone carbon spacing, and processing conditions. These layers have the potential to facilitate decoupled ion transport because the crystalline backbone is relatively immobile.[14,15] Recent work on a precise polyethylene with a sulfonic acid group on every 21st carbon, p21SA, demonstrated excellent proton transport under hydration.[14] The layered assembly of the acid groups enhanced the diffusion of protons compared to more tortuous channels in amorphous proton exchange membranes. Such layered structures may also have a similar benefit for enhanced ion transport in anhydrous single-ion conducting polymer electrolytes for conducting metal cations such as Li^+ or Na^+. The ADMET chemistry presents several challenges, so exploring alternative chemistries for layer-forming functionalized polyethylenes is of key interest.

Precise telechelic polyethylenes, which are short monodisperse end-functionalized polyethylene chains, present an

Received: January 19, 2022
Revised: February 28, 2022
Published: March 14, 2022

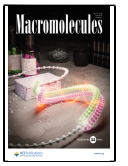

https://doi.org/10.1021/acs.macromol.2c00132
Macromolecules 2022, 55, 2813−2820

opportunity to access layered morphologies with crystalline polymer backbones via alternative chemistries.[18−23] Winey and co-workers recently demonstrated metal ion transport within ionic layers in precise telechelic polyethylenes with carboxylates.[21] However, the reported conductivity values were still quite low compared to traditional SPEs,[1−4] which is primarily due to the carboxylate anions strongly associating to the cations. A high degree of dissociation between the metal cation and tethered anion is critical for decoupled transport within the layered ionic assemblies.[24,25] Sulfonate has a higher degree of dissociation with metal cations than carboxylate,[26] so we are motivated to further study ion transport in layers with SO_3^--containing telechelic polyethylenes. Specifically, we present two precise monodisperse telechelic polyethylenes with 48 carbons and SO_3^- end-functionalization with Li^+ or Na^+, namely $C_{48}(SO_3Li)_2$ and $C_{48}(SO_3Na)_2$. The morphology of $C_{48}(SO_3Na)_2$ nanocrystals in solution has previously been reported.[27] In this work we introduce a new synthesis method and for the first time characterize $C_{48}(SO_3Li)_2$ and $C_{48}(SO_3Na)_2$ as solid polymer electrolytes. We correlate the multiple morphological transitions to ionic conductivity and find an unexpectedly low activation energy for ion transport in $C_{48}(SO_3Na)_2$.

RESULTS AND DISCUSSION

Synthesis. Metal sulfonates are a recurring motif in solid-state electrolytes due to their comparatively high dissociation constant combined with a straightforward synthetic accessibility. While aromatic sulfonates are typically prepared by electrophilic aromatic substitution,[28] aliphatic sulfonates, as targeted here, are accessible by nucleophilic substitution of leaving groups such as aliphatic halides or tosylates with sulfite salts.[19] As a precursor to introduce the C_{48} building block we chose 1,48-octatetracontanediol which is readily accessible by catalytic chain doubling of renewable fatty acids.[20] Additional details regarding the materials used are found in the Supporting Information. From the variety of approaches known to convert hydroxy groups to leaving groups, we found that bromination with PBr_3 in toluene is best suited for this substrate. Because of the presence of two reactive hydroxy end groups, ether side product can form, and this has to be suppressed because they are challenging to separate from the product mixture (Figure 1a). To minimize this reaction pathway, we exploited the strongly temperature-dependent solubility of $C_{48}(OH)_2$ in toluene by applying a slow heating from room temperature to 90 °C to maintain a low concentration of the substrate to be exposed to the excess of PBr_3 reagent. With this approach a selective and virtually quantitative conversion of 98% to the desired 1,48-dibromooctatetracontane ($C_{48}(Br)_2$) was achieved (Figure S1). Soxhlet extraction with chloroform of the finely ground crude product obtained by evaporation of the reaction mixture and subsequent crystallization from the chloroform extracted at 6 °C afforded a 90% yield of pure $C_{48}(Br)_2$.

To overcome the phase separation of the highly hydrophobic $C_{48}(Br)_2$ and the aqueous sodium sulfite reagent solution, a phase transfer catalysis (PTC) with *N*-methyl-*N*,*N*,*N*-trioctyl(decyl)ammonium chloride (Aliquat 336, AQ336) was employed. In our hands, the ionic liquid AQ336 simultaneously served as a phase transfer catalyst, high-temperature lipophilic solvent, and source of bulky quaternary ammonium cations to facilitate workup of the otherwise low-solubility C_{48} disulfonates (Figure 1b). Reacting

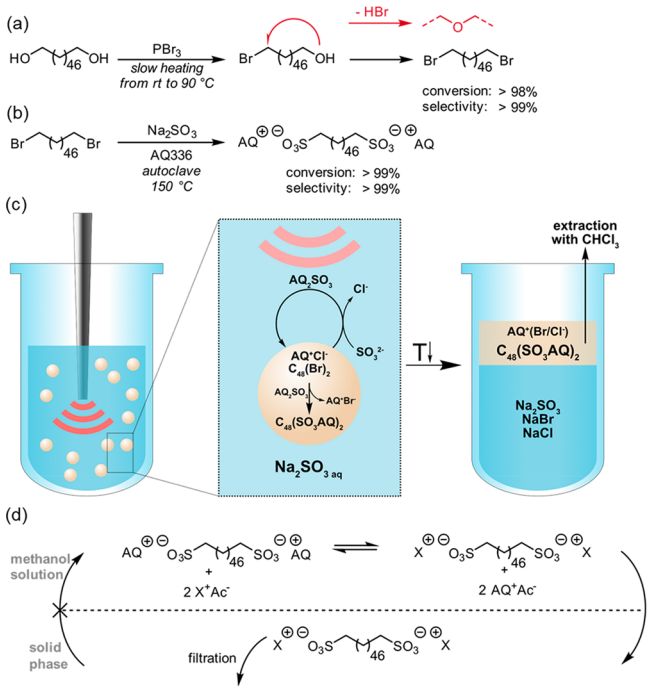

Figure 1. Two-step synthesis of ultralong chain telechelic disulfonates. (a) Bromination of 1,48-octatetracontanediol with PBr_3 via a slow heating ramp to facilitate the selective formation of the α,ω-dibromide without formation of the undesired ether side product. (b) Sulfonation of $C_{48}(Br)_2$. (c) Schematic representation of the reaction of 1,48-dibromooctatetracontane in the presence of a stoichiometric excess of Aliquat 336 as both a phase transfer catalyst cosolvent and a source of bulky counterions simultaneously under high shear. (d) Ion-exchange procedure employing solution of the desired metal counterion in MeOH, where X^+ is Li^+ or Na^+, to make desired $C_{48}(SO_3X)_2$.

this mixture at an elevated temperature of 150 °C in an autoclave facilitated the quantitative conversion of $C_{48}(Br)_2$ to $C_{48}(SO_3AQ)_2$, which could be recovered in an excess of the AQ336 phase by extraction with $CHCl_3$ (see the Supporting Information). The desired metal counterion was then introduced by dropwise injection of the $C_{48}(SO_3AQ)_2$ solution in hot MeOH into saturated methanolic solutions of the respective metal salts and precipitation of the $C_{48}(SO_3Li)_2$ or $C_{48}(SO_3Na)_2$ product (Figure 1d). Recrystallization from MeOH in an autoclave afforded the pure telechelic C_{48} disulfonates.

Thermal Analysis. Differential scanning calorimetry was performed on the $C_{48}(SO_3X)_2$ polymers to identify the thermal transitions (Figure 2). Both $C_{48}(SO_3Li)_2$ and $C_{48}(SO_3Na)_2$ exhibit a melting point (T_m) and crystallization temperature (T_c) as well as additional endothermic/exothermic processes at lower temperatures. The T_m/T_c are 230 °C/220 and 215 °C/195 °C for $C_{48}(SO_3Li)_2$ and $C_{48}(SO_3Na)_2$, respectively. X-ray scattering measurements, as presented below, confirm that these T_m and T_c correspond to crystalline-to-amorphous and amorphous-to-crystalline transitions in the polyethylene backbone. Given that (1) the cations are shared by multiple SO_3^- groups forming secondary bonds between molecules and (2) smaller cations are bound more tightly to the SO_3^- anions, the higher melting temperature in $C_{48}(SO_3Li)_2$ is reasonable.

In $C_{48}(SO_3Li)_2$, a broad thermal transition is present at 125 °C on heating and 105 °C on cooling. In $C_{48}(SO_3Na)_2$, on both heating and cooling, there are several overlapping broad

https://doi.org/10.1021/acs.macromol.2c00132
Macromolecules 2022, 55, 2813−2820

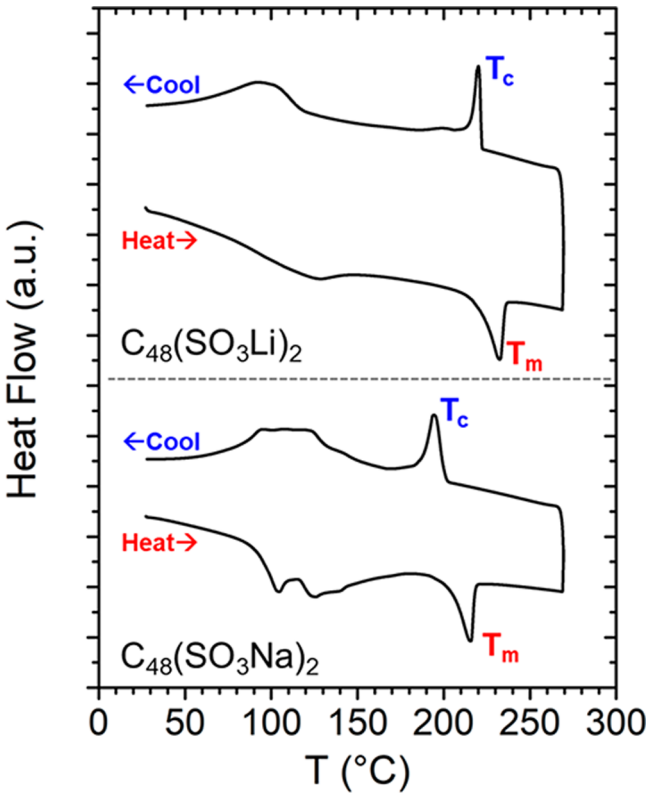

Figure 2. Thermal transitions of $C_{48}(SO_3Li)_2$ and $C_{48}(SO_3Na)_2$ measured by DSC on heating and cooling at a rate of 10 °C/min. Melting (T_m) and crystallization temperatures (T_c) are labeled on both plots.

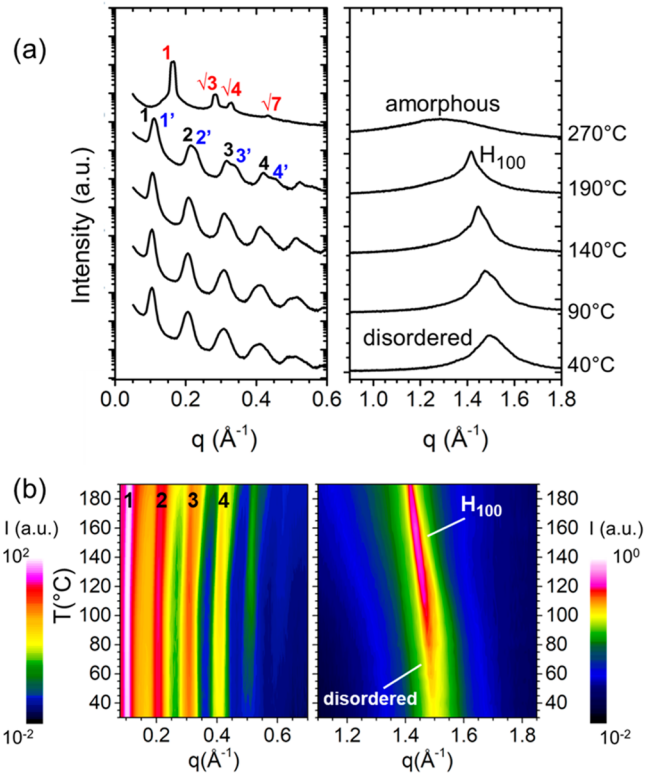

Figure 3. *In situ* small-angle and wide-angle X-ray scattering profiles of $C_{48}(SO_3Li)_2$ at select temperatures during cooling. (a) Data have been shifted vertically, and the intensity is plotted on a log scale (small angle) and linear scale (wide angle), for clarity. Hexagonal ionic assembly peaks ratios are $1:\sqrt{3}:\sqrt{4}:\sqrt{7}$, and layered ionic assembly peaks are 1:2:3:4. Crystal backbone peaks at 190 °C labeled as H_{100} (hexagonal) or as a disordered crystal at 40 °C. (b) Heat map showing all temperatures measured during cooling from 190 to 30 °C (ΔT = 10 °C from 190 to 140 °C; ΔT = 5 °C from 140 to 30 °C). Intensity is on a log scale for all q values. Layer and crystal peaks are labeled consistent with (a).

peaks in the temperature range ~95−160 °C. We attribute these intermediate temperature peaks to various order−order transitions in the backbone structure, which are also present in the $C_{46}(COOX)_2$ telechelic polymers.[21] Although the overlapping peaks in $C_{48}(SO_3X)_2$ are challenging to accurately deconvolute, we identify up to six possible thermal transitions in $C_{48}(SO_3Na)_2$ (Figure S2). We further explore these complex order−order transitions in $C_{48}(SO_3Li)_2$ and $C_{48}(SO_3Na)_2$ via X-ray scattering.

Crystalline Backbone and Layered Assemblies. X-ray scattering was performed on $C_{48}(SO_3Li)_2$ as a function of temperature to identify the backbone morphology and assembly of the functional end groups. Figure 3a illustrates the ordering of the ionic assemblies ($q \sim 0.05-0.6$ Å^{-1}) and the crystal backbone ($q \sim 1.0-1.8$ Å^{-1}) at select temperatures on cooling. Peak positions for the aggregate and backbone regime were determined by fitting with a pseudo-Voigt function (Figure S3). We also note that the structure of $C_{48}(SO_3Li)_2$ is reversible on heating and cooling (Figure S4).

When the backbone is in the melt state, the ionic assemblies ($q \sim 0.05-0.6$ Å^{-1}) exhibit a hexagonal structure, identified by peak ratios of $1:\sqrt{3}:\sqrt{4}:\sqrt{7}$. Upon cooling, $C_{48}(SO_3Li)_2$ exhibits a peak at $q \sim 1.4$ Å^{-1} at 190 °C, which corresponds to the {100} reflection of hexagonally packed polyethylene, labeled H_{100}, with a lattice parameter, a = 5.10 Å. When the polymer crystallizes, the hexagonal ionic assemblies transition into two coexisting sets of ionic layers of similar spacing (60.2 and 56.6 Å at 180 °C), identified by their peak ratios of 1:2:3:4 and 1′:2′:3′:4′.

Figure 3b is a heat map of scattering of the layered ionic assemblies ($q \sim 0.07-0.7$ Å^{-1}) and crystalline backbone ($q \sim 1.1-1.85$ Å^{-1}) from 190 to 30 °C. Upon cooling below T_m, the ionic layers persist as the polyethylene backbone experiences a broad transition from hexagonal crystallinity to a disordered crystal state. The term disordered crystals denotes poorly ordered crystals due to a high density of defects or small crystal size, while exhibiting more local order than the amorphous state. This is consistent with the broad transition detected by DSC measurements upon cooling (Figure 2). Alamo and coworkers found similar disordered crystals in a set of precise, halide-functionalized polyethylenes and a set of precise polyacetals, though their materials were characterized after quenching from the melt.[8,9] In the case of $C_{48}(SO_3Li)_2$, the strong intermolecular interactions associated with cations being shared between the SO_3^- groups hampers the ability of the polymer to crystallize. The steric constraints imposed by the SO_3Li groups disrupt the ability of the hexagonally packed backbone to transition into other crystal structures upon cooling, leaving the backbone a disordered crystal.

X-ray scattering was also performed upon cooling on $C_{48}(SO_3Na)_2$, and selected temperatures are presented (Figure 4). The structure of $C_{48}(SO_3Na)_2$ is reversible on heating and cooling (Figure S5). At 230 °C (above T_c), the backbone is

https://doi.org/10.1021/acs.macromol.2c00132
Macromolecules 2022, 55, 2813−2820

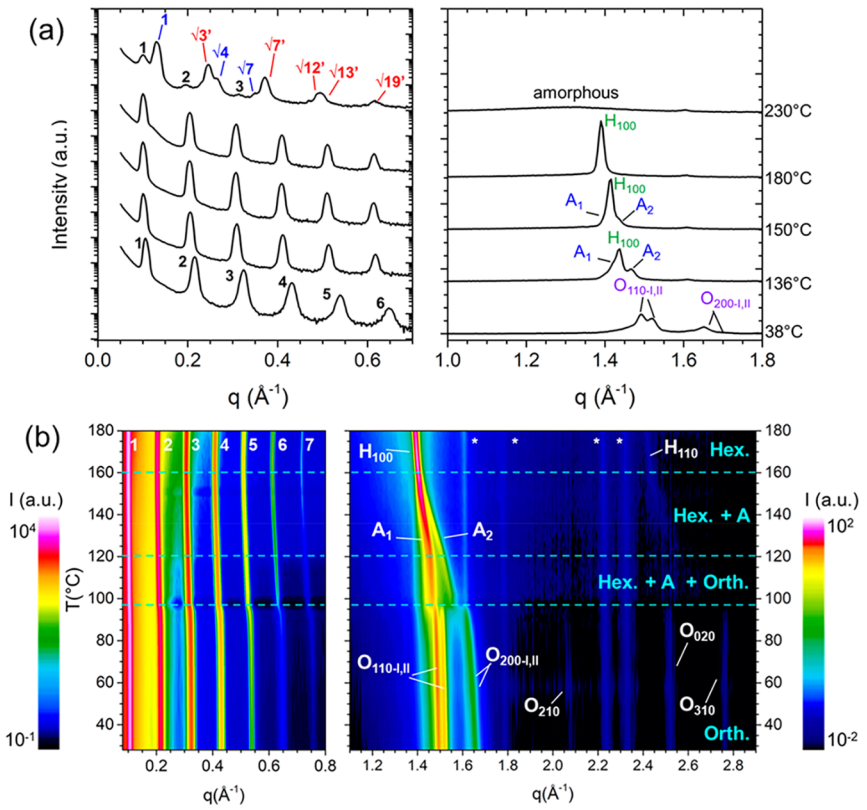

Figure 4. *In situ* small-angle and wide-angle X-ray scattering profiles of $C_{48}(SO_3Na)_2$ at select temperatures during cooling. (a) Data have been shifted vertically, and the intensity is plotted on a log scale (small angle) and linear scale (wide angle), for clarity. Hexagonal aggregate peak ratios are $1:\sqrt{3}:\sqrt{4}:\sqrt{7}$, and layered aggregate peak ratios are 1:2:3:4. Crystal backbone peaks are labeled as H_{100} (hexagonal), A_1 and A_2 (form A), or $O_{110\text{-I,II}}$ and $O_{200\text{-I,II}}$ (orthorhombic structures I and II). (b) Heat map of X-ray scattering profiles (small and wide angle) at all temperatures measured during cooling, from 180 to 28 °C (ΔT = 2 °C from 180 to 88 °C; ΔT = 10 °C from 88 to 28 °C). Intensity is on a log scale for all q values. Layer and crystal peaks are labeled consistent with (a); higher order peaks are also included. The light blue dashed lines indicate approximate order−order transitions, with the backbone morphologies present labeled between each of these temperatures. Weak peaks labeled ∗ are an unknown impurity and do not pose a significant effect on the morphology and ion transport.

amorphous, while the ionic assemblies exhibit a mixture of hexagonally packed and layered morphologies. We note that these coexisting aggregate phases suggest that the system is not fully at equilibrium, and the polymers may be kinetically trapped in a nonequilibrium aggregate morphology. To reach an equilibrium state would likely require heating the polymer to higher temperatures so that the aggregates disorder (at least >300 °C), followed by slow cooling. As the backbone crystallizes, the ionic aggregates form a uniform morphology of layers that persist upon cooling to room temperature, with d_{layer} = 61.4 Å at 180 °C and 58.2 Å at 28 °C. The formation of layered ionic aggregates when the backbone crystallizes and hexagonal aggregates when the backbone is amorphous is consistent with $C_{48}(SO_3Li)_2$ as well as $C_{46}(COONa)_2$.[21]

We further examine the polyethylene backbone of $C_{48}(SO_3Na)_2$ below the crystallization temperature. Although the ionic groups remain assembled in layers upon cooling, the backbone packing exhibits a variety of scattering peaks and coexisting crystal phases. These complex structural transitions in $C_{48}(SO_3Na)_2$ are more clearly seen upon cooling from 180 to 28 °C (Figure 4b). This heat map delineates four temperature ranges based on the crystal phases of the polyethylene backbone. Note that while we specify transitions temperatures, these morphological transitions occur over a range of temperatures at these cooling conditions. Between 180 and 160 °C, the polyethylene backbone of $C_{48}(SO_3Na)_2$ packs into a hexagonal crystal structure (a = 5.22 Å at 180 °C), similar to $C_{48}(SO_3Li)_2$. The hexagonal packing of $C_{48}(SO_3Na)_2$ is more highly ordered than $C_{48}(SO_3Li)_2$, as seen from the narrower H_{100} peak in $C_{48}(SO_3Na)_2$ and the presence of the higher order H_{110} peak at $q \sim 2.4$ Å^{-1} (Figure 4b).

Cooling from 160 to 120 °C, the hexagonal polyethylene crystals coexist with an unknown crystal structure, form A, which exhibits two peaks, A_1 and A_2. The H_{100} and H_{110} peak intensities decrease, while that of A_2 increases, suggesting a transition of some of the hexagonal polyethylene into form A crystals. On the basis of the characteristic lengths of the A_1 and A_2 peaks (Figure S6), it is unlikely that form A is the typical orthorhombic, monoclinic, or hexagonal structure of polyethylene.[21,29,30] Some precisely spaced polyethylenes have been reported to exhibit triclinic crystal structures.[7,8,10,11] The form A crystal could be triclinic, although better crystals would need to be fabricated to provide more conclusive scattering evidence. The coexisting crystal phases suggest that this thermal history produces a nonequilibrium state. These heating and cooling conditions of the X-ray scattering measurements were selected to match those of the electrochemical impedance spectroscopy studies (to be discussed later in further detail). Extended isothermal annealing procedures are required for a more detailed phase analysis, which is beyond the scope of this study.

https://doi.org/10.1021/acs.macromol.2c00132
Macromolecules 2022, 55, 2813−2820

Table 1. Summary of Crystal Structures, Lattice Parameters, Layer Spacing, and Domain Size for $C_{48}(SO_3X)_2$, Measured by X-ray Scattering on Cooling at 180 and 28/30 °C

material	T (°C)	crystal structure	lattice parameter (Å)	areal density (chains nm^{-2})	d_{layer} (Å)	ξ_L (Å)	ξ_C (Å)
$C_{48}(SO_3Li)_2$	180	hex	a = 5.10	4.4	60.2	340	95
					56.6	260	
	30	disordered	--	--	61.7	290	--
$C_{48}(SO_3Na)_2$	180	hex	a = 5.22	4.2	61.4	626	390
	28	orth I	a = 7.59, b = 5.05	5.2	58.2	631	--
		orth II	a = 7.40, b = 4.97	5.4			--
$C_{46}(COONa)_2$[a]	30	orth[a]	a = 7.58, b = 4.81	5.5	59.3	190	--
$C_{46}(COOCs)_2$[a]	30	orth[a]	a = 7.67, b = 4.90	5.3	54.6	233	--

[a]Data for $C_{46}(COOX)_2$ at 30 °C (from ref 21) are included for comparison.

Between 120 and 96 °C, the H_{100} and form A peaks both weaken in intensity and broaden upon cooling, while two coexisting orthorhombic phases begin to appear, O_I and O_{II}. Below 96 °C, there is an abrupt shift in the backbone structure to the orthorhombic phases. We identify two orthorhombic based on their peak positions of $q \sim 1.5$ Å^{-1} and $q \sim 1.65-1.7$ Å^{-1}, corresponding to the orthorhombic (110), $O_{110\text{-}I,II}$, and (200), $O_{200\text{-}I,II}$, reflections, respectively, with lattice parameters listed in Table 1. The presence of two orthorhombic phases may be a result of both the form A and the hexagonal phase transitioning to orthorhombic upon cooling, creating distinct packings in each orthorhombic phase. Higher order peaks are also present for the orthorhombic phases (Figure 4b) although there is insufficient angular resolution to identify O_I or O_{II} for the (210), (020), and (310) reflections. The intermolecular interactions associated with sharing metal cations between SO_3^- groups are stronger for smaller cations. Thus, relative to the Li-neutralized telechelics, the Na-neutralized telechelics have weaker interactions and lower energy barriers associated with the phase transitions, resulting in a lower melting temperature and less defective crystals at low temperatures. The coexisting orthorhombic structures (O_I and O_{II}) illustrate the subtle nature of the energy landscape of these phase transitions.

Table 1 summarizes the key morphological parameters of $C_{48}(SO_3Li)_2$ and $C_{48}(SO_3Na)_2$ at 180 °C and room temperature and compares them to the reported values of $C_{46}(COONa)_2$ and $C_{46}(COOCs)_2$. The $d_{layer} \sim 60$ Å for the sulfonate telechelics is consistent with the layer spacings for $C_{46}(COOX)_2$. The length of 48 all-*trans* carbons is 59 Å, so a certain degree of tilt is expected for $C_{48}(SO_3X)_2$ and $C_{46}(COOX)_2$. Variations in d_{layer} are a result the of the degree of tilt of the telechelic polyethylene, the size of the headgroup, and the mixture of *trans* and *gauche* conformations. The lattice parameters of the polyethylene in the hexagonal regime are similar for $C_{48}(SO_3Li)_2$ and $C_{48}(SO_3Na)_2$ at 180 °C, a = 5.10 and 5.22 Å, respectively. The lattice parameters of the orthorhombic phases in $C_{48}(SO_3Na)_2$ are very similar to those in the carboxylate telechelic ionomers and literature values of standard polyethylene (a = 7.42 Å, b = 4.95 Å).[29] An areal density of chains in the polyethylene crystal was calculated based on the lattice parameters to approximate the areal density of functional groups within the ionic layer; this simplified calculation assumes that the polymers chains are perpendicular to the ionic layers. The hexagonal crystal structure has a lower areal density of functional groups (4.2–4.4 chains nm^{-2}) than the orthorhombic crystal (5.2–5.5 chains nm^{-2}), suggesting more free volume and greater mobility of the tethered SO_3^- head groups in the hexagonal regime.

We estimate the height of the crystallite by using the Scherrer equation, $\xi_L = 2\pi/\Delta q_1$, to determine the correlation length from the layer peak.[16,21] We also estimate the width of the crystallite by using $\xi_C = 2\pi/\Delta q_{H100}$, when a H_{100} crystal peak is clearly evident. Figure 5 illustrates these domain sizes as

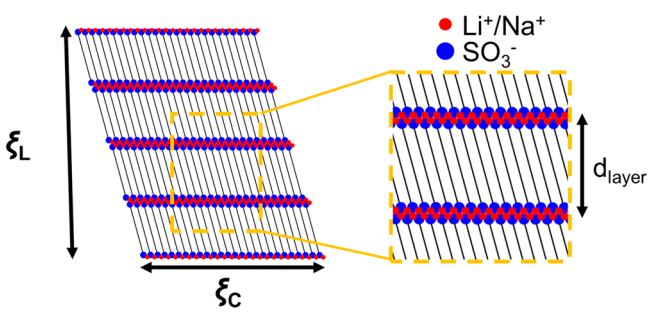

Figure 5. Illustration of layered assemblies in crystallites of telechelic PEs. ξ_L is the approximate height of the crystallite, ξ_C the width of the crystallite, and d_{layer} the spacing between the layered ionic assemblies. The black lines, blue spheres, and red spheres represent the alkyl chains, sulfonate anions, and cationic counterions, respectively.

well as the layer spacing. In $C_{48}(SO_3Li)_2$, $\xi_L \sim 300$ Å when the backbone is hexagonal or disordered, corresponding to an assembly of five repeats of alternating ionic layers and extended polymer chains. This is similar to the $C_{46}(COOX)_2$ telechelic polyethylenes. However, $C_{48}(SO_3Na)_2$ has $\xi_L > 600$ Å, approximately 10 layers thick. Furthermore, ξ_C in the hexagonal backbone regime of $C_{48}(SO_3Na)_2$ is 390 compared to 95 Å in $C_{48}(SO_3Li)_2$, indicating that the assemblies of $C_{48}(SO_3Na)_2$ are approximately 8 times larger. It is not clear exactly what contributes to the formation of larger crystallites, though the lower T_m and T_c in $C_{48}(SO_3Na)_2$ may facilitate larger crystal growth compared to $C_{48}(SO_3Li)_2$, since they were both slowly cooled under similar conditions. Larger crystals correspond to fewer grain boundaries, which can reduce the barriers for ion transport.

Ion Transport. The ionic conductivities, σ_{DC}, of $C_{48}(SO_3Li)_2$ and $C_{48}(SO_3Na)_2$ were determined by using electrochemical impedance spectroscopy (EIS) under vacuum as a function of temperature (Figure 6). The maximum temperature measured was 190 °C, which means the ions are assembled into layered aggregates over the entire range of measurements in both $C_{48}(SO_3Li)_2$ and $C_{48}(SO_3Na)_2$, with the crystal backbone morphologies also denoted in Figure 6. The $C_{48}(SO_3X)_2$ polymers are considered single-ion conductors

https://doi.org/10.1021/acs.macromol.2c00132
Macromolecules 2022, 55, 2813–2820

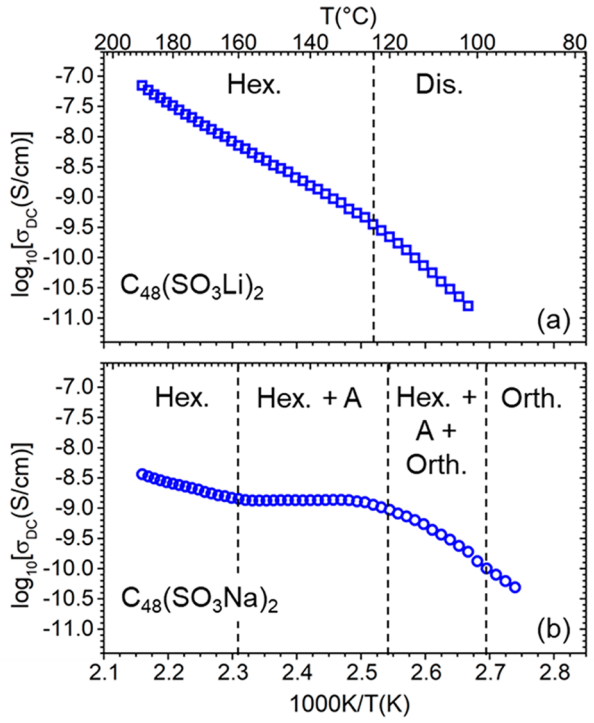

Figure 6. σ_{DC} of (a) $C_{48}(SO_3Li)_2$ and (b) $C_{48}(SO_3Na)_2$, both on cooling as a function of 1000 K/T. Dashed lines correspond to morphological transitions identified by *in situ* X-ray scattering using a comparable cooling protocol. Polyethylene morphologies are labeled, and the ionic groups are assembled in layers at all temperatures.

because the SO_3^- group is covalently bonded to the polymer. The bulk conductivities of $C_{48}(SO_3Li)_2$ and $C_{48}(SO_3Na)_2$ are low compared to traditional single-ion conductors, which is likely due in part to the many interfaces between nanocrystals that would introduce a significant barrier to ion transport. This was similarly reported in the conductivity of the $C_{46}(COOX)_2$ polymers.[21] Many other single-ion conducting polymers are amorphous, without the periodic assemblies or accompanying grain boundaries that exist in these telechelic systems, and typically conduct above T_g or in the melt state, leading to higher ionic conductivities.[31−35] Although the bulk conductivity is low in $C_{48}(SO_3Li)_2$ and $C_{48}(SO_3Na)_2$, we can explore the local ion transport to gain further insight into conductivity mechanisms within the ionic layers.

The ion transport in $C_{48}(SO_3Li)_2$ and $C_{48}(SO_3Na)_2$ exhibits Arrhenius behavior in the high- and low-temperature regimes. The Arrhenius behavior of ion conductivity is described by

$$\sigma_{DC} = \sigma_0 e^{-E_a/RT} \quad (1)$$

where σ_0 is the conductivity at infinite temperature and E_a is the activation energy associated with ion transport. Arrhenius transport is consistent with Li^+ or Na^+ ion transport occurring within the layers and being decoupled from the crystalline backbone. While σ_{DC} characterizes the ion transport throughout the system, E_a informs us of the local ion transport within the ionic layers in the $C_{48}(SO_3X)_2$ polymers (Table 2). Fits to the data in Figure 6 are provided in Figure S7.

We first examine the E_a in the high-temperature regime when the backbones of $C_{48}(SO_3Li)_2$ and $C_{48}(SO_3Na)_2$ are packed hexagonally (Table 2, in bold). The E_a of $C_{48}(SO_3Li)_2$ is 120 kJ mol^{-1}, which is comparable to that of other single Li conductors in the glassy regime with relatively immobile backbones.[3,6] The local ion transport of $C_{48}(SO_3Na)_2$ is significantly improved over $C_{48}(SO_3Li)_2$ when both exhibit hexagonal backbone crystallinity. While the larger cation is expected to have a greater dissociation from the acid group, the very low E_a of 53 kJ mol^{-1} for $C_{48}(SO_3Na)_2$ is quite unexpected, considering other reported single Na-ion conductors have E_a > 85 kJ mol^{-1} or higher.[3,6] The ion transport of $C_{48}(SO_3Na)_2$ is also significantly improved from $C_{46}(COONa)_2$ with hexagonal backbone packing (160 kJ mol^{-1}). A somewhat higher transport is expected in SO_3^- due to better dissociation between the Na^+ with SO_3^- than with COO^-, although the magnitude of the difference in activation energy is surprising. We can also compare the activation energy of hexagonal $C_{48}(SO_3Na)_2$ to that of the precise sulfophenylated polyethylene, p5PhSA-Na, which contains a glassy polymer backbone and disordered percolated aggregates of SO_3Na. In p5PhSA-Na, the E_a of decoupled ion transport is 85 kJ mol^{-1}.[6] The significantly lower E_a of 53 kJ mol^{-1} in hexagonally packed $C_{48}(SO_3Na)_2$ demonstrates the potential of a layered assemblies to be advantageous in future SPEs, compared to materials with disordered assemblies, and highlights the impact that the shape of the ionic assembly may have on decoupled ion transport. We note that a number of other factors besides the ion type and shape of the ionic assemblies could play a role in the low E_a of $C_{48}(SO_3Na)_2$, including the details of the cation coordination with the SO_3^- oxygen atoms and free volume within the system.[5] Both of these factors are a result of local packing of the ions within the layers and merit further investigation using additional experimental techniques or atomistic molecular dynamics simulations.

The E_a of $C_{48}(SO_3Li)_2$ increases from 120 to 183 kJ mol^{-1} as the morphology transitions form hexagonal to disordered crystals at ∼125 °C. In contrast, $C_{48}(SO_3Na)_2$ exhibits an unusual plateau in the conductivity between 120 and 160 °C, which coincides with the presence of the coexisting hexagonal and form A backbone morphologies. This plateau in σ_{DC} appears in both heating and cooling experiments with $C_{48}(SO_3Na)_2$ (Figure S8), as does the coexistence of the hexagonal and form A backbone crystallinity in X-ray scattering. We suspect the plateau in σ_{DC} is a result of the competition between the conductivity in crystals with different backbone morphologies. We conclude that form A promotes ion transport, although the underlying cause for this improvement requires a more thorough understanding of this morphology.

Table 2. Summary of Activation Energy of the $C_{48}(SO_3Li/Na)_2$ Telechelics, with the Corresponding Crystal Backbone Structure and the Temperature Range over Which This E_a Was Determined[a]

material	T range (°C)	backbone morphology	E_a (kJ mol^{-1})
$C_{48}(SO_3Li)_2$	140−190	**hex**	**120**
	<140	dis	183
$C_{48}(SO_3Na)_2$	160−190	**hex**	**53**
	<98	orth	136
$C_{46}(COONa)_2$[a]	130−180	**hex**[a]	**160**
	<130	orth[a]	--
$C_{46}(COOCs)_2$[a]	140−180	**hex**[a]	**92**
	<140	orth[a]	232

[a]Data for $C_{46}(COONa/Cs)_2$ are from ref 21 and included for comparison.

https://doi.org/10.1021/acs.macromol.2c00132
Macromolecules 2022, 55, 2813−2820

The conductivity in $C_{48}(SO_3Na)_2$ decreases more rapidly upon cooling below 120 °C, as the backbone transitions from hexagonal and form A to orthorhombic. Below ∼100 °C, the ion transport again appears Arrhenius, which is consistent with the morphology remaining orthorhombic below this temperature. The E_a in this orthorhombic region is 136 kJ mol^{-1}, which is approximately 2.5 times greater than the E_a of 53 kJ mol^{-1} in the hexagonal packing region in $C_{48}(SO_3Na)_2$, indicating that the hexagonal packing of the backbone is better than orthorhombic for ion transport. A similar result was found in $C_{46}(COOCs)_2$, which has a E_a of 92 kJ mol^{-1} in the hexagonally packed region and an E_a of 232 kJ mol^{-1} in the orthorhombic region.[21] These findings suggest that the lower areal density of functional groups in hexagonally packed crystals relative to orthorhombic crystals can provide more free volume, leading to a lower E_a.

CONCLUSIONS

We have demonstrated that monodisperse telechelic polyethylenes end-functionalized with Li^+ or Na^+ sulfonate form highly ordered layered assemblies that facilitate ion transport when the backbone is crystalline. Both $C_{48}(SO_3Na)_2$ and $C_{48}(SO_3Li)_2$ exhibit hexagonal backbone morphologies upon crystallization from the melt, which is more favorable (lower E_a) for ion transport than the low-temperature disordered or orthorhombic crystals. In $C_{48}(SO_3Na)_2$, there exists an unidentified polyethylene crystal structure, form A, that coexists with the hexagonal backbone structure between 120 and 160 °C, which improves ion transport relative to the hexagonal crystal. The E_a of 53 kJ mol^{-1} $C_{48}(SO_3Na)_2$ when the backbone is hexagonally packed is significantly lower than that of $C_{48}(SO_3Li)_2$ and $C_{46}(COONa)_2$, demonstrating the superior ion transport properties of the Na^+ compared to Li^+ and the SO_3^- anion compared to COO^-. Furthermore, this E_a is lower than that of p5PhSA-Na, which has the same ionic groups assembled into a disordered percolated aggregate morphology. All of these factors demonstrate the potential for layered assemblies to achieve rapid ion transport in crystalline solid polymer electrolytes. While these polymers are polycrystalline materials, it may also be possible to enhance the conductivity by aligning the crystallites and eliminating grain boundaries between the ionic assemblies. Future studies that focus on the local packing *within* the layered aggregate of $C_{48}(SO_3Na)_2$ and explore telechelic or precise polymers with functional groups beyond SO_3^- present opportunities to understand and improve single-ion conduction within layered assemblies.

ASSOCIATED CONTENT

Supporting Information

The Supporting Information is available free of charge at https://pubs.acs.org/doi/10.1021/acs.macromol.2c00132.

Synthesis and characterization methods, intermediate temperature DSC analysis, *in situ* X-ray scattering profiles, EIS Arrhenius fits (PDF)

AUTHOR INFORMATION

Corresponding Authors

Stefan Mecking − *Department of Chemistry, University of Konstanz, 78457 Konstanz, Germany;* orcid.org/0000-0002-6618-6659; Email: stefan.mecking@uni-konstanz.de

Karen I. Winey − *Department of Materials Science & Engineering, University of Pennsylvania, Philadelphia, Pennsylvania 19104, United States;* orcid.org/0000-0001-5856-3410; Email: winey@seas.upenn.edu

Authors

Benjamin A. Paren − *Department of Materials Science & Engineering, University of Pennsylvania, Philadelphia, Pennsylvania 19104, United States;* orcid.org/0000-0002-4361-5182

Manuel Häußler − *Department of Chemistry, University of Konstanz, 78457 Konstanz, Germany*

Patrick Rathenow − *Department of Chemistry, University of Konstanz, 78457 Konstanz, Germany*

Complete contact information is available at: https://pubs.acs.org/10.1021/acs.macromol.2c00132

Funding

K.I.W. and B.A.P. acknowledge funding from the National Science Foundation (NSF) DMR 1904767, NSF PIRE 1545884, and the Vagelos Institute for Energy Science and Technology at the University of Pennsylvania for a graduate fellowship. S.M. and M.H. gratefully acknowledge funding by the Baden-Württemberg Foundation (project "PRICON").

Notes

The authors declare no competing financial interest.

REFERENCES

(1) Manthiram, A.; Yu, X.; Wang, S. Lithium Battery Chemistries Enabled by Solid-State Electrolytes. *Nature Reviews Materials* **2017**, *2* (4), 1−16.

(2) Shaplov, A. S.; Marcilla, R.; Mecerreyes, D. Recent Advances in Innovative Polymer Electrolytes Based on Poly(Ionic Liquid)s. *Electrochim. Acta* **2015**, *175*, 18−34.

(3) Bocharova, V.; Sokolov, A. P. Perspectives for Polymer Electrolytes: A View from Fundamentals of Ionic Conductivity. *Macromolecules* **2020**, *53* (11), 4141−4157.

(4) Diederichsen, K. M.; McShane, E. J.; McCloskey, B. D. Promising Routes to a High Li+ Transference Number Electrolyte for Lithium Ion Batteries. *ACS Energy Letters* **2017**, *2* (11), 2563−2575.

(5) Stacy, E. W.; Gainaru, C. P.; Gobet, M.; Wojnarowska, Z.; Bocharova, V.; Greenbaum, S. G.; Sokolov, A. P. Fundamental Limitations of Ionic Conductivity in Polymerized Ionic Liquids. *Macromolecules* **2018**, *51* (21), 8637−8645.

(6) Paren, B. A.; Thurston, B. A.; Neary, W. J.; Kendrick, A.; Kennemur, J. G.; Stevens, M. J.; Frischknecht, A. L.; Winey, K. I. Percolated Ionic Aggregate Morphologies and Decoupled Ion Transport in Precise Sulfonated Polymers Synthesized by Ring-Opening Metathesis Polymerization. *Macromolecules* **2020**, *53* (20), 8960−8973.

(7) Kaner, P.; Ruiz-Orta, C.; Boz, E.; Wagener, K. B.; Tasaki, M.; Tashiro, K.; Alamo, R. G. Kinetic Control of Chlorine Packing in Crystals of a Precisely Substituted Polyethylene. Toward Advanced Polyolefin Materials. *Macromolecules* **2014**, *47* (1), 236−245.

(8) Zhang, X.; Zuo, X.; Ortmann, P.; Mecking, S.; Alamo, R. G. Crystallization of Long-Spaced Precision Polyacetals I: Melting and Recrystallization of Rapidly Formed Crystallites. *Macromolecules* **2019**, *52* (13), 4934−4948.

(9) Tasaki, M.; Yamamoto, H.; Hanesaka, M.; Tashiro, K.; Boz, E.; Wagener, K. B.; Ruiz-Orta, C.; Alamo, R. G. Polymorphism and Phase Transitions of Precisely Halogen-Substituted Polyethylene. (1) Crystal Structures of Various Crystalline Modifications of Bromine-Substituted Polyethylene on Every 21st Backbone Carbon. *Macromolecules* **2014**, *47* (14), 4738−4749.

(10) Zhang, X.; Zhang, W.; Wagener, K. B.; Boz, E.; Alamo, R. G. Effect of Self-Poisoning on Crystallization Kinetics of Dimorphic Precision Polyethylenes with Bromine. *Macromolecules* **2018**, *51* (4), 1386−1397.
(11) Zhang, X.; Santonja-Blasco, L.; Wagener, K. B.; Boz, E.; Tasaki, M.; Tashiro, K.; Alamo, R. G. Infrared Spectroscopy and X-Ray Diffraction Characterization of Dimorphic Crystalline Structures of Polyethylenes with Halogens Placed at Equal Distance along the Backbone. *J. Phys. Chem. B* **2017**, *121* (43), 10166−10179.
(12) Buitrago, C. F.; Jenkins, J. E.; Opper, K. L.; Aitken, B. S.; Wagener, K. B.; Alam, T. M.; Winey, K. I. Room Temperature Morphologies of Precise Acid-and Ion-Containing Polyethylenes. *Macromolecules* **2013**, *46* (22), 9003−9012.
(13) Buitrago, C. F.; Bolintineanu, D. S.; Seitz, M. E.; Opper, K. L.; Wagener, K. B.; Stevens, M. J.; Frischknecht, A. L.; Winey, K. I. Direct Comparisons of X-Ray Scattering and Atomistic Molecular Dynamics Simulations for Precise Acid Copolymers and Ionomers. *Macromolecules* **2015**, *48* (4), 1210−1220.
(14) Trigg, E. B.; Gaines, T. W.; Maréchal, M.; Moed, D. E.; Rannou, P.; Wagener, K. B.; Stevens, M. J.; Winey, K. I. Self-Assembled Highly Ordered Acid Layers in Precisely Sulfonated Polyethylene Produce Efficient Proton Transport. *Nat. Mater.* **2018**, *17* (8), 1−7.
(15) Trigg, E. B.; Winey, K. I. Nanoscale Layers in Polymers to Promote Ion Transport. *Molecular Systems Design and Engineering* **2019**, *4* (2), 252−262.
(16) Trigg, E. B.; Stevens, M. J.; Winey, K. I. Chain Folding Produces a Multilayered Morphology in a Precise Polymer: Simulations and Experiments. *J. Am. Chem. Soc.* **2017**, *139* (10), 3747−3755.
(17) Baughman, T. W.; Chan, C. D.; Winey, K. I.; Wagener, K. B. Synthesis and Morphology of Well-Defined Poly(Ethylene-Co-Acrylic Acid) Copolymers. *Macromolecules* **2007**, *40* (18), 6564−6571.
(18) Lacombe, J.; Pearson, S.; Pirolt, F.; Norsic, S.; D'Agosto, F.; Boisson, C.; Soulié-Ziakovic, C. Structural and Mechanical Properties of Supramolecular Polyethylenes. *Macromolecules* **2018**, *51* (7), 2630−2640.
(19) Gutfelt, S.; Kizling, J.; Holmberg, K. Microemulsions as Reaction Medium for Surfactant Synthesis. *Colloids Surf., A* **1997**, *128* (1−3), 265−271.
(20) Witt, T.; Häußler, M.; Kulpa, S.; Mecking, S. Chain Multiplication of Fatty Acids to Precise Telechelic Polyethylene. *Angew. Chem. Int. Ed.* **2017**, *56*, 7589−7594.
(21) Yan, L.; Haußler, M.; Bauer, J.; Mecking, S.; Winey, K. I. Monodisperse and Telechelic Polyethylenes Form Extended Chain Crystals with Ionic Layers. *Macromolecules* **2019**, *52* (13), 4949−4956.
(22) Staiger, A.; Paren, B. A.; Zunker, R.; Hoang, S.; Häußler, M.; Winey, K. I.; Mecking, S. Anhydrous Proton Transport within Phosphonic Acid Layers in Monodisperse Telechelic Polyethylenes. *J. Am. Chem. Soc.* **2021**, *143* (40), 16725−16733.
(23) Yan, T.; Guironnet, D. Synthesis of Telechelic Polyolefins. *Polymer Chemistry. Royal Society of Chemistry* **2021**, *12*, 5126−5138.
(24) Tarascon, J.-M.; Armand, M. Issues and Challenges Facing Rechargeable Lithium Batteries. *Nature* **2001**, *414*, 359−367.
(25) Armand, M.; Endres, F.; MacFarlane, D. R.; Ohno, H.; Scrosati, B. Ionic-Liquid Materials for the Electrochemical Challenges of the Future. *Nat. Mater.* **2009**, *8* (8), 621−629.
(26) Zhang, H.; Li, C.; Piszcz, M.; Coya, E.; Rojo, T.; Rodriguez-Martinez, L. M.; Armand, M.; Zhou, Z. Single Lithium-Ion Conducting Solid Polymer Electrolytes: Advances and Perspectives. *Chem. Soc. Rev.* **2017**, *46* (3), 797−815.
(27) Rank, C.; Häußler, M.; Rathenow, P.; King, M.; Globisch, C.; Peter, C.; Mecking, S. Anisotropic Extended-Chain Polymer Nanocrystals. *Macromolecules* **2019**, *52* (16), 6142−6148.
(28) Ma, Q.; Xia, Y.; Feng, W.; Nie, J.; Hu, Y. S.; Li, H.; Huang, X.; Chen, L.; Armand, M.; Zhou, Z. Impact of the Functional Group in the Polyanion of Single Lithium-Ion Conducting Polymer Electrolytes on the Stability of Lithium Metal Electrodes. *RSC Adv.* **2016**, *6* (39), 32454−32461.
(29) Russell, K. E.; Hunter, B. K.; Heyding, R. D. Monoclinic Polyethylene Revisited. *Polymer* **1997**, *38* (6), 1409−1414.
(30) Fontana, L.; Vinh, D. Q.; Santoro, M.; Scandolo, S.; Gorelli, F. A.; Bini, R.; Hanfland, M. High-Pressure Crystalline Polyethylene Studied by x-Ray Diffraction and Ab Initio Simulations. *Physical Review B - Condensed Matter and Materials Physics* **2007**, *75* (17), 1−11.
(31) Paren, B. A.; Raghunathan, R.; Knudson, I. J.; Freyer, J. L.; Campos, L. M.; Winey, K. I. Impact of Building Block Structure on Ion Transport in Cyclopropenium-Based Polymerized Ionic Liquids. *Polym. Chem.* **2019**, *10* (22), 2832−2839.
(32) Fan, F.; Wang, Y.; Hong, T.; Heres, M. F.; Saito, T.; Sokolov, A. P. Ion Conduction in Polymerized Ionic Liquids with Different Pendant Groups. *Macromolecules* **2015**, *48* (13), 4461−4470.
(33) Yan, L.; Rank, C.; Mecking, S.; Winey, K. I. Gyroid and Other Ordered Morphologies in Single-Ion Conducting Polymers and Their Impact on Ion Conductivity. *J. Am. Chem. Soc.* **2020**, *142* (2), 857−866.
(34) Fragiadakis, D.; Dou, S.; Colby, R. H.; Runt, J. Molecular Mobility and Li+ Conduction in Polyester Copolymer Ionomers Based on Poly(Ethylene Oxide). *J. Chem. Phys.* **2009**, *130* (6), 064907.
(35) Choi, U. H.; Liang, S.; O'Reilly, M. v.; Winey, K. I.; Runt, J.; Colby, R. H. Influence of Solvating Plasticizer on Ion Conduction of Polysiloxane Single-Ion Conductors. *Macromolecules* **2014**, *47* (9), 3145−3153.

https://doi.org/10.1021/acs.macromol.2c00132
Macromolecules 2022, 55, 2813−2820